The epigenomic consequences of HDAC6 inactivation reveal a crucial role for P300 suggesting integrated epitherapeutic strategies

Michela Gottardi Zamperla
Istituti Clinici Scientifici Maugeri IRCCS
Barbara Illi
National Research Council (CNR), Sapienza University of Rome
Veronica Barbi
Istituti Clinici Scientifici Maugeri IRCCS
Chiara Cencioni
National Research Council (CNR)-IASI
Daniele Santoni
National Research Council (CNR)-IASI
Stella Gagliardi
IRCCS Mondino Foundation
Maria Garofalo
IRCCS Mondino Foundation
Gabriele Antonio Zingale
IRCCS-Fondazione Bietti
Irene Pandino
IRCCS-Fondazione Bietti
Diego Sbardella
IRCCS-Fondazione Bietti
Lina Cipolla
National Research Council (CNR)
Simone Sabbioneda
National Research Council (CNR)
Antonella Farsetti
National Research Council (CNR)-IASI
Chiara Ripamonti
Italfarmaco Group
Gianluca Fossati
Italfarmaco Group
Christian Steinkühler

Italfarmaco Group
Carlo Gaetano
carlo.gaetano@icsmaugeri.it

Istituti Clinici Scientifici Maugeri IRCCS
Sandra Atlante
National Research Council (CNR)-IASI

Research Article

Keywords: HDAC, HAT, epigenetics, cancer, histone acetylation, proliferation, apoptosis

Posted Date: January 22nd, 2024

DOI: https://doi.org/10.21203/rs.3.rs-3872643/v1

Additional Declarations: Competing interest reported. Italfarmaco SpA, the owner of the ITF3756 commercial rights, employs CP, GF, and CS.

Abstract

Background: Histone deacetylases (HDACs) play a pivotal role in gene regulation, DNA synthesis, and cellular metabolism, significantly influencing cancer development. Class IIb histone deacetylase 6 (HDAC6) is crucial in maintaining protein stability and regulating chromatin dynamics, with notable implications in cancer and immune responses. Despite this, the specific effects of HDAC6 inactivation on gene regulation and chromatin remodeling remain unclear due to the subtle phenotype changes following its genetic deactivation. This study delves into how inactivating HDAC6 affects the stabilization of lysine acetyltransferase P300 and the subsequent impacts on chromatin structure and function in cancer cells.

Methods & Results: Using the HDAC6 inhibitor ITF3756 and CRISPR/Cas9 gene editing, we deactivated HDAC6 in various cancer cell lines. We observed profound changes in chromatin accessibility, particularly in the acetylation of histone H3 lysines 9, 14, and 27, which accumulated into introns and distal intergenic regions as determined through ATAC-seq and H3K27Ac ChIP-seq analyses. Transcriptomics, proteomics, and gene ontology analysis revealed alterations in gene function linked to cell proliferation, adhesion, migration, and apoptosis. A notable finding was the modification of P300 ubiquitination post HDAC6 inactivation, which increased P300 expression and activity, resulting in the downregulation of genes essential for cellular proliferation and survival.

Conclusions: This research underscores the significant effect of HDAC6 inactivation on the chromatin landscape in cancer cells, shedding light on the crucial role of P300 in the HDAC6-mediated anticancer response. Specifically, the role of P300 stabilization in the effectiveness of an HDAC6 inhibitor suggests for a potential shift in focus from HDAC6 to its interaction with P300. This insight could contribute to developing more precise cancer treatments by targeting this specific pathway, thereby enhancing our knowledge of cancer cell behavior and offering new therapeutic perspectives.

Introduction

Histone deacetylases (HDACs) are pivotal in regulating gene expression, DNA synthesis, and cellular metabolism (1). Among them, histone deacetylase 6 (HDAC6) stands out due to its unique structure and multifunctional nature. HDAC6, categorized under class IIb histone deacetylases, boasts two catalytic domains alongside a zinc-finger ubiquitin-binding domain (ZnF-UBP). This structure facilitates its deacetylation functions, targeting several substrates, including α-tubulin (2), cortactin (3), titin (4), and Hsp90 (5), and its ability to bind specific sequences of unanchored ubiquitin, acting as a carrier for transporting aggregated proteins (3, 6–9). While HDAC6 does not directly add ubiquitin chains to proteins, it plays a role in ubiquitination through its interactions with E3 ligases and regulatory functions (10, 11), indirectly affecting protein turnover (10–12). In this context, ubiquitination refers to the conjugation of ubiquitin (Ub) moieties to a lysine residue of the target proteins through a reaction catalyzed by the E1-E2-E3 Ub-conjugating enzymes, with the E3 enzymes conferring substrate specificity (human genome encodes for > 600 E3s) (13). After that, Ub-tagged substrates are generally recognized and digested by the 26S proteasome, a multi-subunit assembly composed of one or two Regulatory

Particles (i.e., the 19S) and a Catalytic Particle (i.e., the 20S) endowed with chymotrypsin-like, trypsin-like and caspase-like activities (13, 14). These mechanisms are essential to maintain cellular homeostasis with potential implications in several pathophysiological conditions, not limited to cancer. They are also relevant for neurodegenerative disorders of the brain and specialized tissues such as the retina and chronic diseases in general (10–12, 15, 16).

Beyond these cellular functions (17), HDAC6 plays a dynamic role in immune regulation, inflammation, and viral infection. Cells utilize HDAC6 modulatory effect on the microtubule transport to assemble and activate inflammasomes (18). Surprisingly, even viruses harness HDAC6 for uncoating during their infection cycle. In this condition, HDAC6 can be a double-edged sword and can thwart viral invasion and replication in a non-enzymatic manner. This versatility links HDAC6 to many diseases, ranging from neurodegenerative conditions to inflammasome-associated ailments, cancer, and viral infections (19, 20).

The transcriptional co-activator lysine acetyltransferase P300 plays a role in several cellular and biological processes, including chromatin remodeling, gene expression, protein turnover, embryonic development, and cell proliferation (10, 21). The concentration of P300 in cells is tightly regulated, and changes in its levels have been observed in various pathophysiological conditions (22, 23). Specifically, P300 might undergo polyubiquitination and sumoylation in regions near the bromodomain, and these post-translational modifications are often associated with its unphosphorylated form (10, 21, 24).

Various signaling pathways, including the MAP kinase p38 and the Ras pathway, can influence P300 degradation or stabilization (10, 25). Moreover, post-translational modifications such as phosphorylation, ubiquitination, and interactions with other proteins can also play a role in determining P300 subcellular localization. Specific signaling pathways and molecular interactions would likely be involved in these regulatory processes, affecting P300's ability to act as a transcriptional co-activator or its other functions within the cell (21, 25, 26).

Previous research suggests that P300 interacts with and acetylates HDAC6, attenuating HDAC6 deacetylase activity (27). This relationship underscores a complex interplay between acetylation and deacetylation processes in cells, with P300 modulating chromatin structure and transcriptional activities, such as that of Sp1 and other transcription factors, but also the function of epigenetic enzymes, including HDAC6 activity (6, 28, 29).

The physical interplay between HATs and HDACs, both present in the regulatory domains of target genes, is crucial for controlling gene expression. Employing specific HDAC inhibitors can help re-establish the disrupted acetylation equilibrium observed in various pathophysiological conditions such as cancer, respiratory, or cardiac diseases.

Notably, the selective inhibition of HDAC6 does not show cytotoxic effects in healthy cells or mice (27, 30). Developing isoform-selective HDAC inhibitors allows tailored therapeutic applications in cancer, inflammatory, and infectious diseases (1, 31). Given the implications of HDAC6 in various pathophysiological conditions and its potential therapeutic significance, several small molecule inhibitors

have been developed primarily targeting its deacetylase activity (32). In this direction, the recently described compound ITF3756 is a potent and selective HDAC6 inhibitor with a favorable pharmacokinetic profile. It demonstrates low toxicity both *in vitro* and *in vivo*. Furthermore, ITF3756 has been shown to increase the function of regulatory T cells, suggesting its potential employment in treating autoimmune diseases, in applications related to organ transplantation, or modulating the anticancer immune response (33). Additionally, severe viral infections, including COVID-19, ITF3756, and other HDAC inhibitors, might provide therapeutic benefits by modulating harmful inflammatory pathways and reducing cytokine storms (34, 35).

Despite the elevated level of characterization, the consequences of HDAC6 interaction with P300 are barely understood (11, 28, 29). This manuscript explores the role of HDAC6 as a modulator of P300 expression and function and the epigenomic consequences of selective HDAC6 targeting in cancer cells (31).

Materials and Methods

An extended Materials & Methods section is available as supplemental information.

Cell culture, treatment, and transfection. HCC1806 (CRL-2335, *Homo Sapiens*, breast cancer), MDA-MB-231 (CRM-HTB-26, *Homo Sapiens*, breast cancer), Jurkat (Clone E6-1, TIB-152, H*omo Sapiens*, Acute leukemia, T-lymphocyte), MRC5 (CCL-171, *Homo Sapiens*, fetal lung, fibroblast) and WI-38 (CCL-75, *Homo Sapiens*, fetal lung, fibroblast) cell lines were purchased from ATCC; B16-F10 WT line and KO line for HDAC6 were purchased from genOwa (*Mus Musculus*, skin melanoma, a mixture of spindle-shaped and epithelial-like cells).

Crystal violet staining. After treatment, cells were fixed in fresh 2% paraformaldehyde (PFA) at room temperature (RT) for 20 minutes (min) and stained with 0,5% Crystal violet solution (methyl violet 10B or hexamethyl pararosaniline chloride, prepared in 20% methanol) at RT for 5 min, washed with phosphate-buffered saline (PBS) and dried for 30 min.

ELISA assays. Total HDAC and HAT activity were assayed on nuclear and cytoplasmic extracts obtained using the Nuclear Extraction Kit (ab113474, Abcam), following the manufacturer's instructions. Total HDAC activity was quantified using the HDAC Activity Assay Kit (colorimetric, ab1432, Abcam), and total HAT activity was quantified using the Histone Acetyltransferase Activity Assay Kit (colorimetric, ab65352, Abcam) according to the supplier protocols.

mRNA extraction and qRT-PCR. According to the manufacturer's instructions, RNA was extracted from approximately 1x106 cells using Tri-Reagent (Sigma). cDNA synthesis for quantitative real-time PCR (qRT-PCR) was retrotranscribed with Omniscript RT Kit (Qiagen). All reactions were performed in RT² SYBR Green ROX qPCR Mastermix (Qiagen), using the QIAquant 96 5plex (230V) Device (Qiagen).

Immunoprecipitation and capillary electrophoresis. Cells were lysed in 20 mM Tris-HCl (pH 7.4), 50 mM NaCl, 1% NP40/IGEPAL, 2 mM EDTA, 0.01% SDS, supplemented with protease/phosphatase inhibitor (PI/PhI) mix and 2 mM DTT and protein concentration was determined by a BCA kit. 500 µg of the extract was immunoprecipitated by using 5 µg of anti-P300 (RbMAb, Abcam), anti-HDAC6 (MsMAb, Abcam), or anti-Flag (MsMAb, Abcam) and Dynabeads-Protein G magnetic beads system (Thermofisher Scientific).

Protein extraction from mice tissue. Samples were cut into small pieces with a scalpel and transferred into tubes. To each tube, two 3mm Tungsten Carbide Beads and Leammli buffer supplemented with 100 nM Phenylmethanesulfonyl fluoride (PMSF, Merk), 100 µM Trichostatin A (TSA, Cabru-Cayman Chemical) and PI/PhI mix were added. Samples were loaded to TissueLyzer LT and shaken 3–6 times for 3 min at 50 Hz; after centrifugation, samples were heated at 95°C and sonicated to avoid DNA interference.

Immunofluorescence staining. Treated/untreated HCC1806 cells and WT and KO_HDAC6 B16F10 cells were cultured in LabTek II chamber slides (Nunc, Biosigma) and fixed in 4% PFA (Merck) for 10 min, RT, and permeabilized with 0.1% Triton solution (Merck) for 30 min at RT. Samples were blocked in 5% BSA for 90 min, incubated overnight at 4°C with primary antibodies, and 1h at RT with secondary antibodies.

Proximity ligation assay (PLA). MCR5 cells were transfected with hHDAC6-Flag-pcDNA3.1+ (Aurogene) and treated with ITF3756 at 1 µM for 16h. Cells were then fixed with 4% PFA for 15 min, RT, permeabilized with 0.5% Triton X-100 for 20 min at RT, and blocked with 3% BSA–PBS 0.1% Tween for 1h at 37°C. After that, samples were incubated with P300 (1:200, RbMAb, Abcam) and Flag (1:200, MsMAb, Abcam) for two h at 37°C and washed with PLA Buffer A (Sigma), and a classic PLA reaction was performed by using the SIGMA Duolink Kit, according to the manufacturer instructions.

Proteasome Assay. Vehicle and ITF3756-treated samples were lysed in an osmotic buffer according to a standard procedure for isolating crude cell extracts (36)—protein concentration determined by BCA assay. After that, 20 µg of proteins were incubated 10 min at 37°C with or without 1 µM epoxomicin, a potent and irreversible inhibitor of proteasome chymotrypsin-like activity (Boston Biochem, MA, USA). 75 µM Suc-LLVY-amc (Boston Biochem, MA, USA) was added, and the fluorescence released by proteasome cleavage was recorded in a Varioskan Lux spectrofluorometer ($\lambda_{exc.}$ = 340 nm; $\lambda_{em.}$ = 440 nm). Slopes for individual samples were calculated by subtracting that observed in the presence of epoxomicin.

Western blotting. Cell lysed in Laemmli buffer 1X supplemented with 1 mM DTT. Thereafter, 4–20% acrylamide pre-cast gels (Bio-Rad, Hercules, CA, USA) were used to separate proteins by SDS-PAGE. After separation, proteins were transferred to a HyBond-ECL nitrocellulose filters (Bio-Rad, Hercules, CA, USA) and probed with antibodies for several targets (37).

Assay for Transposase-Accessible Chromatin (ATAC) sample preparation. B16F10 KO_HDAC6 and WT cells and ITF3756 and DMSO treated Jurkat cells were cultured for 16h, then treated for 30 min at 37°C with 1x DNase buffer (200 units/mL in HBSS, 2.5 mM $MgCl_2$, 0.5 mM $CaCl_2$). 10^5 cells were then cryopreserved in 50% FBS, 40% growth media, 10%DMSO, frozen, and sent to Active Motif (Carlsbad, CA, USA) for analysis.

ATAC sequencing and bioinformatics analysis. The paired-end 42 bp sequencing reads (PE42) generated by Illumina sequencing were mapped to the genome using the BWA algorithm with default settings ("bwa mem"). Only reads that passed Illumina purity filter, aligned with no more than 2 mismatches, and mapped uniquely to the genome were used in the subsequent analysis. In addition, duplicate reads ("PCR duplicates") were removed. Genomic regions with high transposition/tagging events were determined using the MACS3 peak calling algorithm (Zhang et al., Genome Biology 2008, 9: R137).

Chromatin immunoprecipitation (ChIP) sample preparation. ITF3756 and DMSO treated Jurkat cells, and B16F10 KO_HDAC6 and WT cells were cultured for 16h, then cross-linked with 1% formaldehyde solution (10 mM NaCl, 100 µM EDTA pH 8.0, 5 mM HEPES, pH 7.9) and quenched with 120 mM Glycine. Samples were then treated with 0.5% Igepal supplemented with 1 mM PMSF, pelleted, snap frozen, and sent to Actif Motif (Carlsbad, CA, USA) for H3K27Ac-ChIP-seq analysis (anti-H3K27Ac, Cat# 39133).

ChIP sequencing and bioinformatics analysis. ChIP samples were processed for sequencing, and the 75-nt single-end (SE75) sequence reads generated by Illumina sequencing are mapped to the genome using the BWA algorithm ("bwa aln/samse" with default settings). Only reads that passed the Illumina purity filter, aligned with no more than 2 mismatches, and mapped uniquely to the genome were used in the subsequent analysis. In addition, duplicate reads ("PCR duplicates") were removed. Since the 5´-ends of the aligned reads (= "tags") represent the end of ChIP/IP-fragments, the tags are extended in silico (using Active Motif software) at their 3´-ends to a length of 200 bp, which corresponds to the average fragment length in the size-selected library.

Bioinformatics analysis of NGS studies. Volcano plots were computed using GraphPad Prism 8 to identify regions of interest in the ATAQ-seq (Differentially accessible regions (DARs) *vs* Differentially inaccessible regions) and the ChIPSeq (upregulated H3K27Ac targeted regions *vs* downregulated H3K27Ac targeted regions) applying the following threshold to identify statistically significant regions modulated by pharmacological treatment or HDAC6 KO: ±1 log2 fold change, fdr < 0.05.

RNA Library preparation, sequencing, and bioinformatics analysis. Sequencing libraries were prepared with the Illumina TruSeq Stranded RNA Library Prep, version 2, Protocol D, using 500-ng total RNA (Illumina). 4200 Tape Station assessed the quality of each library with a "DNA High sensitivity" assay (Agilent). Libraries were fluorometrically quantified using a Sensitivity dsDNA assay with a Qubit device (Life Technologies). The sequencing step was performed with NGS technologies using Illumina Genome Analyzer and the NextSeq 500/550 High Output v2.5 kit (150 cycles) (Illumina), processed on Illumina NextSeq 500. FastQ files were generated via Illumina bcl2fastq2, version 2.17.1.14. Available online: http://support.illumina.com/downloads/bcl-2fastq-conversion-software-v217.html (accessed on 2 May 2018, starting from raw sequencing reads produced by Illumina NextSeq sequencer).

Proteomics Studies. The proteome characterization of HDAC6-silenced and scrambled (treated with a non-targeting pool of siRNA) HCC1806 cells was performed using a standard shot-gun proteomics protocol. Peptides were analyzed by LC/MS-MS in Orbitrap Exploris 240 (Thermo Fisher Scientific, Waltham, MA, USA) online with a nano ultra-high-pressure liquid chromatography system (Dionex,

Ultimate 3000). Analysis was done in Label-Free Quantification mode and Data Dependent Acquisition (DDA). Raw files were then analyzed by Proteasome Discoverer (2.5), and proteins identified by Sequest-HT coupled with Percolator against a human UniProt database (UP000005640–9606, containing 82685 entries). A contaminant list was included in the analysis. Carbamidomethylation of cysteine was set as static modification, whereas acetylation and ubiquitination were set as variable modification at lysine residues with phosphorylation ad serine or threonine residues. FDR was set at 0.01, and targets were validated using a concatenated target-decoy strategy. Proteins discussed in the results were filtered for the following parameters: i) Identification with at least 2 peptides and 1 unique peptide; ii) Identification in at least 50% of samples belonging to the same experimental group.

Statistical analysis. Statistical analyses were performed using the GraphPad Prism program.

Results

HDAC6 modulation influences the growth rate of cancer cells.

Several cancer cell lines were treated at a range of ITF3756 from 250 nM to 5 µM. Cell growth was monitored over 72h (Fig. S1 A-D). At 48h, crystal violet staining showed a marked reduction in HC1806 triple-negative breast cancer and B16F10 melanoma cell proliferation (Fig. S1 E-F) at concentrations equal to or greater than 1 µM. HDAC6 inactivation by CRISPR-Cas9 in B16F10 cells confirmed the inhibitory effect of HDAC6 inhibition on cell proliferation. Fig. S2 A highlights a 20% growth decrease in HDAC6_KO cells compared to WT. Furthermore, the HDAC6-deprived cells exhibited a dampened and scattered growth pattern concerning WT cells and enhanced response to the 5 µM ITF3756 treatment (Fig. S2 B).

HDAC6 modulation influences lysine acetylation dynamics.

Remarkable changes in several acetylation markers were observed when HCC1806 cells were treated with 1 µM ITF3756 for 16h. Immunofluorescence staining established a 2- to 6-fold increase in the acetylation levels of H3K27, H3K9, and H3K14. In contrast, the levels of H4K16Ac decreased (Fig. 1A-B, Fig. S3 A-B). These observations were validated by capillary electrophoresis analyses, which demonstrated an enrichment in the acetylation levels of H3K4Ac post-treatment. However, H3K23Ac was not modulated (as seen in Fig. S3 C). This pattern of acetylation after ITF3756 treatment was consistent across other cell lines, including human and mouse triple-negative breast cancer cell lines MDA-MB-231 (Fig. S4 A) and 4T1 (Fig. S4 B), as well as the human leukemia T-lymphocyte Jurkat cell line (Fig. S4 C). It is worth noting that the non-tumorigenic pulmonary Wi38 fibroblasts exhibited a different acetylation pattern (Fig. S4 D). Different results emerged in the HDAC6_KO cells. Immunofluorescence staining revealed a 2-fold enhancement in the acetylation levels of H3K27, H3K9, and H3K14 in the HDAC6-inactivated cells compared to their wild-type counterparts. Meanwhile, a decline in the H4K16Ac signal was recorded (Fig. 1. C-D, Fig. S5 A-B). These findings were supported by capillary electrophoresis analyses, which showed a similar enrichment in acetylation markers, including H3K4Ac, H3K9Ac, H3K14Ac, and H3K27Ac, while H3K23Ac and H4K16Ac remained relatively stable (Fig. S5 C). When the B16F10 wild-type cells

were exposed to 1 µM ITF3756 for 16h, they mirrored the acetylation profiles observed in the HDAC6-inactivated cells, with significant increases, especially in H3K4Ac, H3K9Ac, H3K14Ac, and H3K27Ac histone markers (Fig. S5 D). The effects of HDAC6 modulation are not limited to histone lysine modifications. They also extend to the acetylation of K40 on α-tubulin, a well-known target of HDAC6. Indeed, ITF3756 induced a pronounced increase in α-tubulin acetylation, as determined by both immunofluorescence and capillary electrophoresis, in several cell lines (Fig. S6 A-E).

HDAC6 inactivation impacts lysine acetylation in vivo.

We took advantage of HDAC6_KO mice to validate what was observed *in vitro.* Specific acetylation markers, including α-tubulin K40, H3K9, H3K14, H3K27, and H4K16, were investigated in both WT and HDAC6_KO mice by using capillary electrophoresis performed on tissue extracts from various organs, including liver, spleen, brain, and heart. There was a significant increase in K40 acetylation in liver, spleen, and heart samples. However, the same result did not occur in the brain (Fig. S6 F). In livers from HDAC6_KO mice, an increased acetylation of H3 on lysine 9 and 27 was detected (Fig. 1E). Conversely, H3K14 and H4K16 did not change in HDAC6_KO animals. (Fig. S7 A). In the spleen, acetylation of K27 on histone H3 was higher in HDAC6_KO mice (Fig. 1F), while H3K9, H3K14, and H4K16 did not change (Fig. 1F and S7 B). Neither the brain nor the heart showed any considerable modification in histone acetylation levels (Fig. S7 C-D).

HDAC6 inhibition/inactivation increases global HAT activity and elevated P300 protein levels.

To delve deeper into the effects of ITF3756, we explored whether any changes were detectable in total HDAC and total HAT activities upon HDAC6 inhibition/inactivation. HCC1806 cells treated with ITF3756 1 µM for 16h showed no alteration in total HDAC activity compared to the control (Fig. S8 A, left panel). This result indicates that other HDACs might compensate for the loss of HDAC6 function or that a reduction in HDAC6 activity is insufficient to determine appreciable changes in global HDAC activity. However, there was a remarkable increase in global HAT activity in the ITF3756 conditions compared to the control solvent (Fig. 2A). Interestingly, global levels of acetyl-CoA (AcCoA), which serves as the substrate for HATs, remained unchanged (Fig. S8 A, right panel), suggesting that the effect of HDAC6 inhibition on total HAT activity was not dependent on an altered metabolism of AcCoA. To get more insights, we evaluated whether P300, one of the most abundant HAT within cells and known to interact with HDAC6 (28), was affected by ITF3576 treatment. When we assessed the mRNA expression levels of HDAC6 and P300, we found no significant difference upon ITF3756 treatment (Fig. S8 B), hinting that ITF3756 did not transcriptionally impact HDAC6 and P300 functions. However, capillary electrophoresis experiments showed increased P300 protein levels, as depicted in Figs. 2B and 2C, whereas HDAC6 protein levels were not modulated. A similar result was observed when HDAC6 was inactivated using siRNAs, leading to a decrease in HDAC6 expression by around 70% and a 2-fold increase of P300 protein levels (Fig. 2D). Noteworthy, P300 inactivation, using siRNAs, did not change HDAC6 levels (Fig. S9 A), while treating si_P300 HCC1806 cells with ITF3756 1 µM for 16h, P300 protein levels increased, once again, significantly (Fig. 2E), leading to relatively higher levels of H3K9Ac and H3K27Ac (Fig. S9 B).

Additionally, total HAT activity and P300 protein levels were notably higher in HDAC6_KO than in WT cells (Fig. 2F and G). Nevertheless, total HDAC activity, AcCoA levels, and P300 mRNA levels did not change (Fig. S8 C-D).

Comparable results were obtained in ITF3756-treated Jurkat (Fig. S8 E-F) and B16F10 cells (Fig. S8 G-H).

Of note, P300 inhibition by the small molecule EML425 (38), lead to a significant decrease in H3K9Ac and H3K27Ac levels in HCC1806 cells before and after HDAC6 inactivation by siRNAs (Fig. S9 C)

HDAC6 inhibition promotes P300 stabilization.

HEK293T cells were transfected with pcDNA3.1+-HDAC6-Flag and control pcDNA3.1+ (empty vector, EV). After 24h, cells were exposed to 1 μM ITF3756 for an additional 16h, and co-immunoprecipitation experiments, analyzed by capillary electrophoresis, were performed to assess whether a putative HDAC6/P300 complex could dissociate in the presence of ITF3576 (Fig. 3A). We found that in this cellular system, HDAC6-Flag content did not change after treatment, and the transfected protein was mainly localized in the cytoplasm in both conditions (Fig. 3B). On the contrary, there was an evident increase in P300 levels in treated samples (Fig. 3A, B and Fig. S9 D). Furthermore, the enzyme appeared to be predominantly localized in the nucleus of ITF3576-treated cells than in controls. Moreover, we detected an HDAC6/P300 complex in untreated cells, significantly reduced after ITF3756 administration.

Proximity Ligation Assays (PLA) further confirmed these findings (Fig. S9 D). Indeed, in pcDNA3.1+-HDAC6-Flag-transfected MRC5 cells, a significant interaction was observed between the endogenous P300 and transfected HDAC6-Flag. This interaction was more pronounced than in the control cells expressing EV alone. Moreover, P300 levels increased upon ITF3576 treatment in pcDNA3.1 + and pcDNA3.1+-HDAC6-Flag transfected cells, as previously observed. A decrease in PLA signal was detected upon normalization of PLA foci on P300 content in pcDNA3.1 + and pcDNA3.1+-HDAC6-Flag-transfected cells upon ITF3576 treatment. (Fig S9 D, bottom right graph). These experiments support the evidence that P300 can be associated with HDAC6, whereas HDAC6 inhibition reduces this interaction while increasing P300 protein levels.

We then investigated which mechanism could support the increase in P300 protein levels detected upon ITF3576 treatment. Since P300 might undergo polyubiquitination and HDAC6 was reported to serve a role in Ub-signaling mechanisms, we evaluated whether HDAC6 inhibition could change the rate of P300 ubiquitination. To this aim, HCC1806 cells were exposed to 1 μM ITF3756 for 16h, and immunoprecipitation with an anti-polyubiquitin antibody was performed (Fig. 3C). We observed a significant reduction in the polyubiquitinated species of P300 in the ITF3756-treated cells, compared to controls, despite the marked increase in P300 (Fig. 3C, bottom right).

To corroborate further the specificity of this observation and to rule out that P300 stabilization was not caused by global alterations of proteasome or Ub-signalling induced by ITF3756, canonical parameters

of UPS activity were assayed in HCC1806 treated with 1 μM ITF3756 for 16h and compared to controls (i.e., solvent-treated).

Crude cell extracts (i.e., the soluble fraction of cytosol) were isolated under non-denaturing conditions from ITF3756- and solvent-treated cells and assayed for the rate of cleavage of the fluorogenic probe LLVY-amc by the chymotrypsin-like activity of intact proteasome particles. The spectrofluorimetric assay is commonly called proteasome assay (see Methods). The slopes of each sample were then calculated over a linear interval. The data highlighted that the rate of cleavage of LLVY-amc (expressed as μmol/min) was fully comparable between ITF3756- and solvent-treated cells (Fig. S10A), suggesting that the drug did not alter the basal proteasome activity.

To strengthen this finding, the same extracts were further analyzed by Wb. Filters were assayed for the overall content of *i*) representative proteasome subunits, either belonging to the 20S (i.e., PSMA7, PSMB6) and the 19S (i.e., PSMD4); *ii*) Ub-proteins and those conjugated with Ub-K:48 linkages, which more truthfully identify proteasome substrates (i.e., the K:48 topology of Ub-chains is the preferential configuration for substrate processing through the 26S proteasome) (Fig. S10B).

Also, in this case, the data obtained after normalization suggested that the overall content in proteasome subunits and Ub-proteins was fully comparable between ITF3756- and solvent-treated cells.

Therefore, the overall data set suggests that ITF3756 treatment, reducing HDAC6/P300 association, might inhibit P300 ubiquitination through its stabilization.

HDAC6 inactivation affects chromatin accessibility.

Transposase-accessible chromatin sequencing (ATAC-seq) assay and H3K27Ac chromatin immunoprecipitation sequencing (ChIP-seq) were performed on B16F10 HDAC6_KO and WT cell lines. Indeed, Principal Component Analysis (PCA) shows HDAC6_KO and WT cells well separated in both analyses (Fig. S11-S12 A).

ATAC-seq and H3K27Ac-ChIP-seq experiments revealed a significant number of differentially accessible regions (DARs) with a $-0.5 \leq$ shrunken LogFC ≤ 0.5 and p adjusted-value ≤ 0.05 (Fig. S11-S12 B). Specifically, 4835 DARs were identified from the ATAC-seq and 9650 DARs from the ChIP-seq.

For what concern the genomic features, the majority of different ATAC and H3K27Ac peaks between HDAC6_KO and WT samples occurred at introns and distal intergenic regions (Fig. S11-S12 C), red and green bars, respectively). The GO analysis revealed putative targets of HDAC6 inactivation (Fig. S11-S12 D). These analyses highlighted a different regulation of genes involved in cell proliferation (GO-ID: 0008283), cell adhesion (GO-ID: 0007155), and migration (GO-ID: 0016477), which were down-modulated due to inaccessible chromatin (Fig. S11-S12 D, left panel, blue bars). Meanwhile, genes with a role in apoptotic pathways (GO-ID: 0043065) were up-regulated due to increased chromatin accessibility (right graphs, red bars, in Fig. S11-S12 D). Specifically, by combining the HDAC6-associated DARs, identified by ATAC-seq and ChIP-seq analyses, two protein networks related to down- and up-regulated regions,

respectively, were generated, pointing out a series of genes associated with an altered survival program including *Akt1, Itgb3, Gas6, Sox9, Nf1, Tgfb2*, and *Casp7* (Fig. 4A and B).

Similar results were obtained by analyzing Jurkat cells treated with 1 μM ITF3756 for 16h compared to solvent controls by ATAC-seq and H3K27ac-ChIP-seq. The PCA showed that the two samples were well separated (Fig. S13-S14 A); the ATAC-seq revealed 1399 DARs and the ChIP-seq 11450 DARs with a -0.5 ≤ shrunken LogFC ≤ 0.5 and p adjusted-value ≤ 0.05 (Fig. S13-S14 B). Again, the most affected genomic features were the introns and the distal intergenic regions (Fig. S13-S14 C, red and green bars, respectively). Once more, the GO analyses showed a different regulation in the biological processes related to cell proliferation, cell adhesion, and apoptosis (Fig. S13-S14 D).

The effect of HDAC6 inactivation in B16F10 cells has been further assessed by comparing the KO_HDAC6 and the WT condition by transcriptome analysis. Genes with − 1 ≤ Log2FC ≤ 1 and p adjusted-value ≤ 0.1 were considered differentially expressed (DE) and retained for further analysis. Through DESeq2 analysis, it was possible to identify 554 up- and 778 down-regulated genes in the KO_HDAC6 condition. The PCA analysis distinguishes the two conditions (Fig. S15 A). The volcano plot highlighted all statistically significant DE genes in the two subgroups; the expression difference is considered significant for a -1 ≤ Log2FC ≤ 1 and p adjusted-value ≤ 0.1. Red dots represent significantly up- and downregulated genes with 1 ≤ Log2FC ≤ 1 (*x*-axis) and a p adjusted-value ≤ 0.1 (*y*-axis; Fig. S15 B). The 60 most modulated genes were selected and represented in the heatmap, in which the cluster genes, separated according to their degree of modulation, could be observed. KO_HDAC6 samples appeared to have different gene expression profiles than WT controls (Fig. S15 C). To further explore the mechanisms underlying the differences observed between the two groups, GO term enrichment analysis for DE genes DE_KO_HDAC6_*vs*_WT was performed for both up-regulated and down-regulated genes. In the dot-plot graph, results are represented according to the criterion for which the red dots are the most significantly differentially regulated; while the point size indicates the number of genes involved in the process, the dot position represents the expression fold change. The biological processes, the cell components, the molecular functions, and the KEGG pathways analyses of KO_HDAC6 samples revealed a significant modulation in genes correlated with the extracellular matrix, cell adhesion, cell motility, regulation of protein stability, channel activity, signal transduction, and receptor complexes (Fig. S15 D-G).

Of note, the change in the expression of some of the genes associated with an altered survival program (*Casp7, Sox9, Smad 3, Itgb3, Nf1*, and *Tgfb2*) was validated by RT-qPCR (Fig. S15 H).

Furthermore, proteomic analyses were performed on HCC1806 scramble and HDAC6-silenced cells. Among the 3010 proteins identified (Fig. 16A, B), the gene ontology analysis of upregulated or downregulated proteins between HDAC6-silenced and scrambled cells revealed a significant modulation (Log2FC = 0.58 and p adjusted-value ≤ 0.05 (Benjamini-Hochberg correction). Specifically, also in this condition, from the GO analysis, we observed modulation in proteins related to the process of cell proliferation (GO-ID:0008283), cell adhesion(*e.g.* GO-ID: 0007155), cell migration(GO-ID: 0016477),

extracellular matrix organization (GO-ID: 0030198), channel activity and integrin binding (*e.g.* GO-ID: 0005178, Fig. S16 C-H) confirming the data provided by the transcriptomic analyses on HDAC6_KO B16F10 cells.

Discussion

The interplay between HDACs and HATs maintains a balanced acetylation homeostasis within the cell. The acetylation and deacetylation of histones and non-histone proteins, orchestrated by HATs and HDACs, respectively, are crucial for regulating cellular function, chromatin structure, and gene expression. Indeed, the action of HDAC inhibitors can indirectly favor the actions of HATs by tipping the balance towards a more acetylated and transcriptionally active chromatin state. Therefore, the therapeutic effects observed with HDAC inhibitors might reflect, at least in part, the broader impact on the acetylation landscape within the cell, which is a result of the interplay between HDACs and HATs (39).

Notably, some evidence indicates that in the presence of an HDAC pan-inhibitor, P300 results stabilized (40). HDAC inhibitors stimulate HAT autoacetylation and enhance P300 HAT activity, facilitating the acetylation of histones and other proteins, thus impacting gene expression. Autoacetylation also affects P300 interaction with other proteins and their stability, playing a significant role in various cellular processes and disease states (41). In this direction, Trichostatin A, the most well-characterized HDAC pan-inhibitor, has been found to promote P300 stabilization and lysine acetylation on some substrates, including transcription factors, signaling proteins, or structural histones (40, 42). This effect has been associated with P300 autoacetylation and association with specific targets, including the retinoic acid receptor alpha or the kinase HIPK2 (43). However, the role of HDAC6 in this context remains unclear.

Interestingly, SIRT2, a class III HDAC, has been implicated in P300 deacetylation, and sirtuin inhibitors have been reported to increase HAT activity, stabilizing P300. Although HDAC6 interacts with SIRT2, it does not seem involved in the P300 deacetylation/acetylation balance and stabilization (44, 45). Conversely, the association of P300 with HDAC6 has been implicated in the negative regulation of HDAC6 lysine deacetylation function (28, 29).

At nanomolar or in the lower micromolar (1–2 μM) range of concentrations, the IT3756 inhibitor has a selective affinity for HDAC6 (35). It is well tolerated and works in cells derived from different primary tumors. In such conditions, we found that the total HDAC activity is virtually unchanged, suggesting that the compound does not significantly impact the most active HDACs, possibly including class I. However, we noticed a remarkable increase in histone H3 lysine acetylation in all tested conditions, particularly on Lysine 9, 14, and 27. This effect has been associated with stabilizing P300 protein levels paralleled by a significant increase in acetylase activity.

We found that a cytoplasmic HDAC6 /P300 complex, constitutively present in the control condition, dissociates in the presence of ITF3756. The molecular basis of this process is poorly characterized, but changes in the HDAC structural conformation following the inhibitor binding might account for it (37). In this direction, it is well documented that HDAC inhibitors, including those selective for HDAC6 such as

Tubacin, disrupt HDAC6 protein complexes with some functional consequences. In the case of HDAC6::PP1 complexes, the release of HDAC6 determined by an HDAC inhibitor increased PP1 activity (38). In our experiments, ITF3756 caused the dissociation of HDAC6 from P300 with consequent protein stabilization and an increase in total HAT activity. This phenomenon is associated with a significant enrichment in lysine acetylation on histone H3. This effect has been observed in all the conditions tested, including cells treated with the ITF3756 inhibitor and transfected with siRNA or in which HDAC6 has been genetically inactivated.

Interestingly, in HDAC6 KO mice, we observed an enrichment of acetylated histone H3, particularly in the liver and the spleen, but not in the heart and the brain. The reason for this distribution is unclear; however, we may consider that the heart and the brain have limited abilities to proliferate, while the liver and the spleen can proliferate in response to regenerative stimuli or infections. Intriguingly, in the case of DNA methylation, it has been reported that the heart and brain accumulate more methylated cytosines than organs with a higher proliferative verve (46, 47).

A more precise understanding of the changes induced by HDAC6 inactivation originates from the bioinformatic analyses. The bioinformatics undertaken in this study centered on evaluating the impact of HDAC6 inactivation on gene expression profiles and chromatin accessibility, offering critical insights into the molecular dynamics within cancer cells (48). The Gene Ontology (GO) analysis was instrumental in identifying gene regulation shifts, particularly in cell proliferation, adhesion, and migration domains. The down-regulation of genes in these categories, due to decreased chromatin accessibility, underscores a potential mechanistic pathway through which HDAC6 inactivation contrasts cancer cell growth and dissemination (49). This reduced accessibility likely reflects a more condensed chromatin state, hindering the transcriptional machinery's access to crucial oncogenic regions (50).

Conversely, the up-regulation of genes implicated in apoptotic pathways presents an equally significant aspect of HDAC6 inactivation. This phenomenon suggests chromatin relaxation in regions governing apoptotic processes, potentially facilitating the transcription of genes that drive programmed cell death. This shift towards apoptosis is particularly interesting: it indicates a possible therapeutic leverage point: promoting apoptosis in cancer cells, which remains a pivotal strategy in oncology (51). This observation is fostered further by the ATAC-seq and ChIP-seq combined analyses, which deepened the understanding of these epigenetic changes. This analysis highlighted specific genes crucial in cell survival programs, such as *Akt1, Itgb3, Gas6, Sox9, Nf1, Tgfb2*, and *Casp7*. Each of these genes plays a vital role in the cellular circuitry, and their modulation could have profound implications for cancer cells' survival, proliferation, and metastatic potential. For instance, the down-modulation of *Akt1*, a key signaling molecule in many cellular processes, including the cell cycle and survival, might directly impact the viability and aggressiveness of cancer cells. Similarly, the negative regulation of SRY-box transcription factor 9 (*Sox9*), known for its role in cell fate determination and tumorigenesis, could impact cancer cell differentiation and invasive potential (52).

In addition to providing insights into the direct effects of HDAC6 inactivation, these findings also indicate potential biomarkers for the response to HDAC6 inhibitors. The specific genes identified could be monitored to gauge the efficacy of HDAC6-targeted therapies and might help tailor treatments to individual patients based on their tumor molecular profile from a precision medicine perspective. Furthermore, the differential regulation of these genes hints at the potential synergistic effects that could be achieved by combining HDAC6 inhibitors with other therapeutic agents. For example, targeting the AKT pathway with HDAC6 inhibition might yield enhanced anti-tumor effects in cancers where this pathway is aberrantly activated (53, 54).

Moreover, the global changes in chromatin accessibility and gene expression patterns offer a broader perspective on the role of HDAC6 in the epigenetic regulation of cancer cells. This role encompasses the direct deacetylation activities of HDAC6 and its wider influence on the epigenetic landscape, affecting gene expression indirectly through chromatin remodeling. Intriguingly, the epigenome reshaping properties of HDAC6 cannot be separated by the function of P300. This crucial acetylase is stabilized by HDAC6 inhibition and, promoting lysine acetylation such as the H3K27Ac enrichment, contributes to some of the chromatin changes observed in this study (55–57). This aspect of HDAC6 function could have far-reaching implications, considering the emerging importance of multi-targeted epigenetic therapies in cancer treatment (58). In this direction, the bioinformatic analyses in this study provide a view of the molecular alterations induced by HDAC6 inactivation. These results expand our understanding of the complex interplay between epigenetic regulation and cancer cell biology and underscore the potential of HDAC6 as a therapeutic target in various cancers (59).

In conclusion, the findings described in this manuscript underscore the significant potential of the ITF3736 inhibitor in epigenetic modulation. By disrupting the association between HDAC6 and P300, the inhibitor ITF3736, or other strategies, not only stabilizes P300 but also amplifies total HAT activity and global histone acetylation. This property is further evidenced by the diminished ubiquitination of P300, supporting its enhanced stability and sustained cellular activity. Concurrently, the enrichment of histone H3 acetylation on lysines, especially at lysine 27, offers insights into the broader transcriptional implications of this interaction. The modulation of the HDAC6-P300 dynamic could pave the way for novel treatments in diseases where the epigenetic control over chromatin structure and protein function is broadly compromised.

Declarations

Ethics approval and consent to participate: N/A.

Consent for publication: All authors agreed to this publication.

Availability of data and material: The datasets generated or analyzed during the current study are not publicly available due to their consideration in a patenting process but are available from the corresponding author on a reasonable request.

Author Contributions: MGZ and BI conceived and carried out experiments and data analysis and revised the manuscript; CC and DS carried out the bioinformatics analysis; VB, LC, MG, GAZ, IP carried out experiments; CC, SG, SS, DS, AF, CR, GF, CS revised data analysis and the manuscript; CG and SA conceived the experiments and wrote the manuscript. All the authors contributed critical discussion and approved the final version of the manuscript.

Competing Interest Statement: CP, GF, and CS are employed by Italfarmaco SpA, the owner of the ITF3756 commercial rights.

Funding

This work has been supported by the Ministry of Health and Fondazione Roma to DS. The Italian Ministry of University and Research and EU funding within the MUR PNRR "National Center for Gene Therapy and Drugs based on RNA Technology" (Project no. CN00000041 CN3 RNA) and by the Italian National Research Council (CNR), progetti@cnr.it (IMMUNAGE) to AF. CG, CS, and GF were supported by progetto “ImmunHUB” Regione Lombardia.

Acknowledgments: None.

References

1. Milazzo G, Mercatelli D, Di Muzio G, Triboli L, De Rosa P, Perini G, et al. Histone Deacetylases (HDACs): Evolution, Specificity, Role in Transcriptional Complexes, and Pharmacological Actionability. Genes (Basel). 2020;11(5).
2. Hubbert C, Guardiola A, Shao R, Kawaguchi Y, Ito A, Nixon A, et al. HDAC6 is a microtubule-associated deacetylase. Nature. 2002;417(6887):455–8.
3. Zhang X, Yuan Z, Zhang Y, Yong S, Salas-Burgos A, Koomen J, et al. HDAC6 modulates cell motility by altering the acetylation level of cortactin. Mol Cell. 2007;27(2):197–213.
4. Lin YH, Major JL, Liebner T, Hourani Z, Travers JG, Wennersten SA, et al. HDAC6 modulates myofibril stiffness and diastolic function of the heart. J Clin Invest. 2022;132(10).
5. Kovacs JJ, Murphy PJ, Gaillard S, Zhao X, Wu JT, Nicchitta CV, et al. HDAC6 regulates Hsp90 acetylation and chaperone-dependent activation of glucocorticoid receptor. Mol Cell. 2005;18(5):601–7.
6. Fusco C, Micale L, Augello B, Mandriani B, Pellico MT, De Nittis P, et al. HDAC6 mediates the acetylation of TRIM50. Cell Signal. 2014;26(2):363–9.
7. Li L, Yang XJ. Tubulin acetylation: responsible enzymes, biological functions and human diseases. Cell Mol Life Sci. 2015;72(22):4237–55.
8. Li Y, Shin D, Kwon SH. Histone deacetylase 6 plays a role as a distinct regulator of diverse cellular processes. FEBS J. 2013;280(3):775–93.

9. Yang Y, Rao R, Shen J, Tang Y, Fiskus W, Nechtman J, et al. Role of acetylation and extracellular location of heat shock protein 90alpha in tumor cell invasion. Cancer Res. 2008;68(12):4833–42.
10. Sadoul K, Boyault C, Pabion M, Khochbin S. Regulation of protein turnover by acetyltransferases and deacetylases. Biochimie. 2008;90(2):306–12.
11. Xu Y, Wan W. Acetylation in the regulation of autophagy. Autophagy. 2023;19(2):379–87.
12. Pernet L, Faure V, Gilquin B, Dufour-Guerin S, Khochbin S, Vourc'h C. HDAC6-ubiquitin interaction controls the duration of HSF1 activation after heat shock. Mol Biol Cell. 2014;25(25):4187–94.
13. Komander D, Rape M. The ubiquitin code. Annual review of biochemistry. 2012;81:203–29.
14. Livneh I, Cohen-Kaplan V, Cohen-Rosenzweig C, Avni N, Ciechanover A. The life cycle of the 26S proteasome: from birth, through regulation and function, and onto its death. Cell research. 2016;26(8):869–85.
15. Zhu Y, Feng M, Wang B, Zheng Y, Jiang D, Zhao L, et al. New insights into the non-enzymatic function of HDAC6. Biomed Pharmacother. 2023;161:114438.
16. Abouhish H, Thounaojam MC, Jadeja RN, Gutsaeva DR, Powell FL, Khriza M, et al. Inhibition of HDAC6 Attenuates Diabetes-Induced Retinal Redox Imbalance and Microangiopathy. Antioxidants. 2020;9(7).
17. Valenzuela-Fernandez A, Cabrero JR, Serrador JM, Sanchez-Madrid F. HDAC6: a key regulator of cytoskeleton, cell migration and cell-cell interactions. Trends Cell Biol. 2008;18(6):291–7.
18. Tsujimoto K, Jo T, Nagira D, Konaka H, Park JH, Yoshimura SI, et al. The lysosomal Ragulator complex activates NLRP3 inflammasome in vivo via HDAC6. EMBO J. 2023;42(1):e111389.
19. Kulthinee S, Yano N, Zhuang S, Wang L, Zhao TC. Critical Functions of Histone Deacetylases (HDACs) in Modulating Inflammation Associated with Cardiovascular Diseases. Pathophysiology. 2022;29(3):471–85.
20. Seidel C, Schnekenburger M, Dicato M, Diederich M. Histone deacetylase 6 in health and disease. Epigenomics. 2015;7(1):103–18.
21. Chen J, Li Q. Life and death of transcriptional co-activator p300. Epigenetics. 2011;6(8):957–61.
22. Ghosh AK. Acetyltransferase p300 Is a Putative Epidrug Target for Amelioration of Cellular Aging-Related Cardiovascular Disease. Cells. 2021;10(11).
23. Sun H, Yang X, Zhu J, Lv T, Chen Y, Chen G, et al. Inhibition of p300-HAT results in a reduced histone acetylation and down-regulation of gene expression in cardiac myocytes. Life Sci. 2010;87(23–26):707–14.
24. Lu P, Xu Y, Sheng ZY, Peng XG, Zhang JJ, Wu QH, et al. De-ubiquitination of p300 by USP12 Critically Enhances METTL3 Expression and Ang II-induced cardiac hypertrophy. Exp Cell Res. 2021;406(1):112761.
25. Girdwood D, Bumpass D, Vaughan OA, Thain A, Anderson LA, Snowden AW, et al. P300 transcriptional repression is mediated by SUMO modification. Mol Cell. 2003;11(4):1043–54.

26. Sankar N, Baluchamy S, Kadeppagari RK, Singhal G, Weitzman S, Thimmapaya B. p300 provides a corepressor function by cooperating with YY1 and HDAC3 to repress c-Myc. Oncogene. 2008;27(43):5717–28.
27. Bobrowska A, Paganetti P, Matthias P, Bates GP. Hdac6 knock-out increases tubulin acetylation but does not modify disease progression in the R6/2 mouse model of Huntington's disease. PLoS One. 2011;6(6):e20696.
28. Han Y, Jeong HM, Jin YH, Kim YJ, Jeong HG, Yeo CY, et al. Acetylation of histone deacetylase 6 by p300 attenuates its deacetylase activity. Biochem Biophys Res Commun. 2009;383(1):88–92.
29. Liu Y, Peng L, Seto E, Huang S, Qiu Y. Modulation of histone deacetylase 6 (HDAC6) nuclear import and tubulin deacetylase activity through acetylation. J Biol Chem. 2012;287(34):29168–74.
30. Getsy PM, Coffee GA, Kelley TJ, Lewis SJ. Male histone deacetylase 6 (HDAC6) knockout mice have enhanced ventilatory responses to hypoxic challenge. Res Sq. 2023.
31. Dallavalle S, Pisano C, Zunino F. Development and therapeutic impact of HDAC6-selective inhibitors. Biochem Pharmacol. 2012;84(6):756–65.
32. Zhao Y, Liang T, Hou X, Fang H. Recent Development of Novel HDAC6 Isoform-selective Inhibitors. Curr Med Chem. 2021;28(21):4133–51.
33. Beier UH, Akimova T, Liu Y, Wang L, Hancock WW. Histone/protein deacetylases control Foxp3 expression and the heat shock response of T-regulatory cells. Curr Opin Immunol. 2011;23(5):670–8.
34. Ripamonti C, Spadotto V, Pozzi P, Stevenazzi A, Vergani B, Marchini M, et al. HDAC Inhibition as Potential Therapeutic Strategy to Restore the Deregulated Immune Response in Severe COVID-19. Front Immunol. 2022;13:841716.
35. Vergani B, Sandrone G, Marchini M, Ripamonti C, Cellupica E, Galbiati E, et al. Novel Benzohydroxamate-Based Potent and Selective Histone Deacetylase 6 (HDAC6) Inhibitors Bearing a Pentaheterocyclic Scaffold: Design, Synthesis, and Biological Evaluation. J Med Chem. 2019;62(23):10711–39.
36. Elsasser S, Schmidt M, Finley D. Characterization of the proteasome using native gel electrophoresis. Methods Enzymol. 2005;398:353–63.
37. Sbardella D, Tundo GR, Coletta M, Manni G, Oddone F. Dexamethasone Downregulates Autophagy through Accelerated Turn-Over of the Ulk-1 Complex in a Trabecular Meshwork Cells Strain: Insights on Steroid-Induced Glaucoma Pathogenesis. Int J Mol Sci. 2021;22(11).
38. Milite C, Feoli A, Sasaki K, La Pietra V, Balzano AL, Marinelli L, et al. A novel cell-permeable, selective, and noncompetitive inhibitor of KAT3 histone acetyltransferases from a combined molecular pruning/classical isosterism approach. J Med Chem. 2015;58(6):2779–98.
39. Slaughter MJ, Shanle EK, Khan A, Chua KF, Hong T, Boxer LD, et al. HDAC inhibition results in widespread alteration of the histone acetylation landscape and BRD4 targeting to gene bodies. Cell Rep. 2021;34(3):108638.
40. Kim SH, Kang HJ, Na H, Lee MO. Trichostatin A enhances acetylation as well as protein stability of ERalpha through induction of p300 protein. Breast Cancer Res. 2010;12(2):R22.

41. Jain S, Wei J, Mitrani LR, Bishopric NH. Auto-acetylation stabilizes p300 in cardiac myocytes during acute oxidative stress, promoting STAT3 accumulation and cell survival. Breast Cancer Res Treat. 2012;135(1):103–14.
42. Ryan CM, Harries JC, Kindle KB, Collins HM, Heery DM. Functional interaction of CREB binding protein (CBP) with nuclear transport proteins and modulation by HDAC inhibitors. Cell Cycle. 2006;5(18):2146–52.
43. Choi JR, Lee SY, Shin KS, Choi CY, Kang SJ. p300-mediated acetylation increased the protein stability of HIPK2 and enhanced its tumor suppressor function. Sci Rep. 2017;7(1):16136.
44. Black JC, Mosley A, Kitada T, Washburn M, Carey M. The SIRT2 deacetylase regulates autoacetylation of p300. Mol Cell. 2008;32(3):449–55.
45. Han Y, Jin YH, Kim YJ, Kang BY, Choi HJ, Kim DW, et al. Acetylation of Sirt2 by p300 attenuates its deacetylase activity. Biochem Biophys Res Commun. 2008;375(4):576–80.
46. Bachman M, Uribe-Lewis S, Yang X, Burgess HE, Iurlaro M, Reik W, et al. 5-Formylcytosine can be a stable DNA modification in mammals. Nat Chem Biol. 2015;11(8):555–7.
47. Bachman M, Uribe-Lewis S, Yang X, Williams M, Murrell A, Balasubramanian S. 5-Hydroxymethylcytosine is a predominantly stable DNA modification. Nat Chem. 2014;6(12):1049–55.
48. Zhang QQ, Zhang WJ, Chang S. HDAC6 inhibition: a significant potential regulator and therapeutic option to translate into clinical practice in renal transplantation. Front Immunol. 2023;14:1168848.
49. Li T, Zhang C, Hassan S, Liu X, Song F, Chen K, et al. Histone deacetylase 6 in cancer. J Hematol Oncol. 2018;11(1):111.
50. Grandi FC, Modi H, Kampman L, Corces MR. Chromatin accessibility profiling by ATAC-seq. Nat Protoc. 2022;17(6):1518–52.
51. Jo H, Shim K, Jeoung D. Targeting HDAC6 to Overcome Autophagy-Promoted Anti-Cancer Drug Resistance. Int J Mol Sci. 2022;23(17).
52. Aguilar-Medina M, Avendano-Felix M, Lizarraga-Verdugo E, Bermudez M, Romero-Quintana JG, Ramos-Payan R, et al. SOX9 Stem-Cell Factor: Clinical and Functional Relevance in Cancer. J Oncol. 2019;2019:6754040.
53. Iida M, Harari PM, Wheeler DL, Toulany M. Targeting AKT/PKB to improve treatment outcomes for solid tumors. Mutat Res. 2020;819–820:111690.
54. Pascual J, Turner NC. Targeting the PI3-kinase pathway in triple-negative breast cancer. Ann Oncol. 2019;30(7):1051–60.
55. Jin Q, Yu LR, Wang L, Zhang Z, Kasper LH, Lee JE, et al. Distinct roles of GCN5/PCAF-mediated H3K9ac and CBP/p300-mediated H3K18/27ac in nuclear receptor transactivation. EMBO J. 2011;30(2):249–62.
56. Wang M, Chen Z, Zhang Y. CBP/p300 and HDAC activities regulate H3K27 acetylation dynamics and zygotic genome activation in mouse preimplantation embryos. EMBO J. 2022;41(22):e112012.

57. Cai LY, Chen SJ, Xiao SH, Sun QJ, Ding CH, Zheng BN, et al. Targeting p300/CBP Attenuates Hepatocellular Carcinoma Progression through Epigenetic Regulation of Metabolism. Cancer Res. 2021;81(4):860–72.
58. Benedetti R, Conte M, Iside C, Altucci L. Epigenetic-based therapy: From single- to multi-target approaches. Int J Biochem Cell Biol. 2015;69:121–31.
59. Kaur S, Rajoria P, Chopra M. HDAC6: A unique HDAC family member as a cancer target. Cell Oncol (Dordr). 2022;45(5):779–829.

Figures

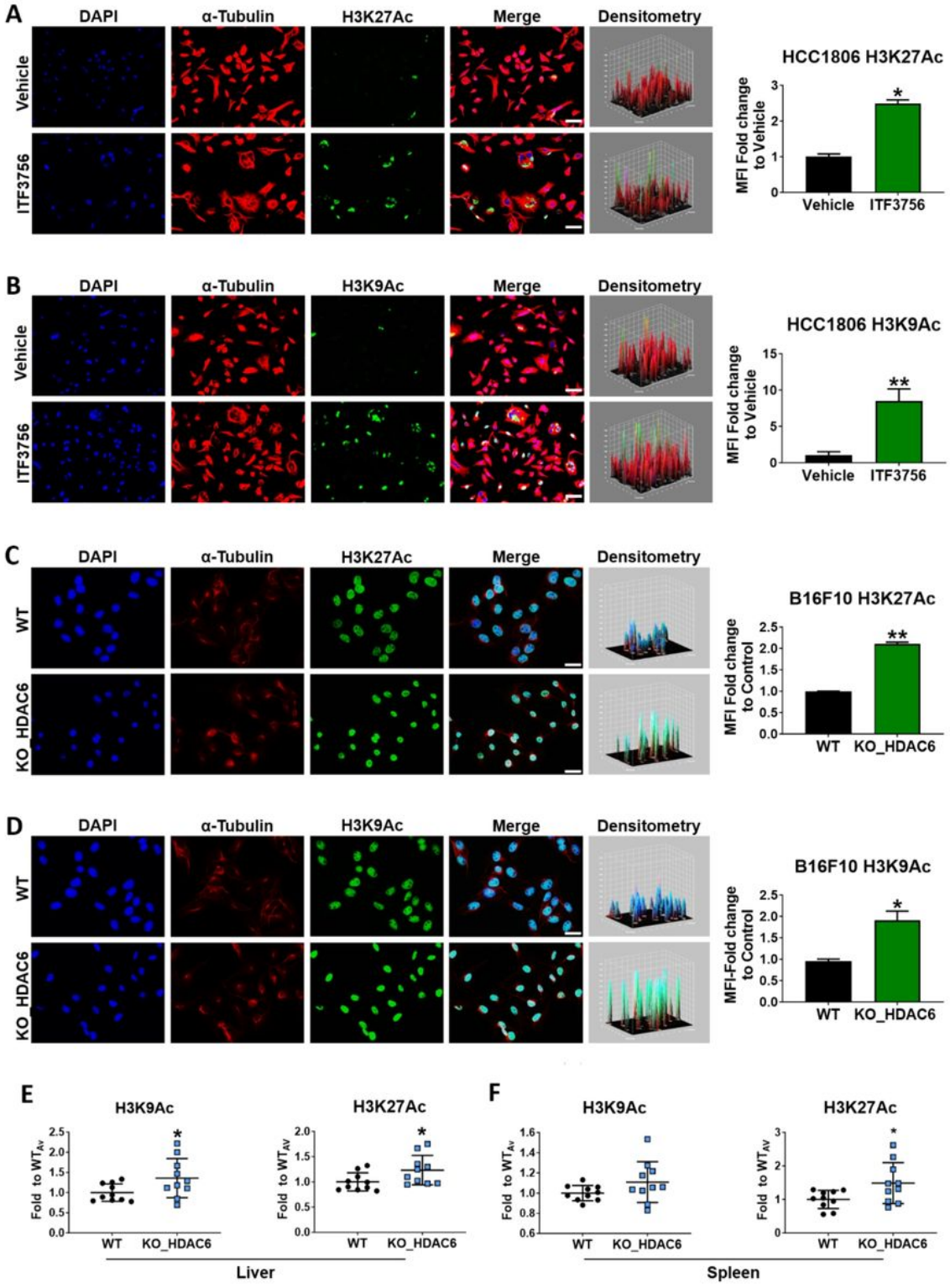

Figure 1

HDAC6 inhibitor ITF3756 and HDAC6 inactivation by CRISPR/CAS9 modulate lysine acetylation. (**A, B**) Immunofluorescence staining after ITF3756 treatment of HCC 1806 cell line. Left: representative images showing the acetylation of H3K27 (**A**) and H3K9 (**B**) (green signal) after 16h treatment with ITF3756 1 μM. DAPI (blue signal) and α-Tubulin (red signal) were normalizers. Images were acquired at 20X magnification. Scale bar: 100 μm. Right: densitometric analysis of the Mean Fluorescent Intensity (MFI)

of the ITF3756 treated cells (green bar) compared to solvent (black bar). Error bars indicate SEM. Data were analyzed by paired t-test, N=3; *p<0.05; **p<0.005. (**C, D**) Immunofluorescence staining of B16F10 KO_HDAC6 *vs* WT. Left: representative images showing the acetylation of H3K27 (**C**) and H3K9 (**D**) (green signal). DAPI (blue signal) and α-Tubulin (red signal) were normalizers. Images acquired at 40X magnification. Scale bar: 50 μm. Right: densitometric analysis of the Mean Fluorescent Intensity (MFI) of the KO_HDAC6 condition (green bar) compared to the control (black bar). Error bars indicate SEM. Data were analyzed by unpaired t-test, N=3; *p<0.05; **p<0.005. (**E, F**) The graphs show the results of capillary electrophoresis experiments performed to detect H3K9 and H3K27 acetylation in the liver (**E**) and spleen (**F**) of HDAC6_KO mice (blue dots) compared to the control (WT, black dots). The β-Actin was used as a normalizer. Error bars indicate SD. Data were analyzed by unpaired t-test, N=10 for each condition; *p<0.05.

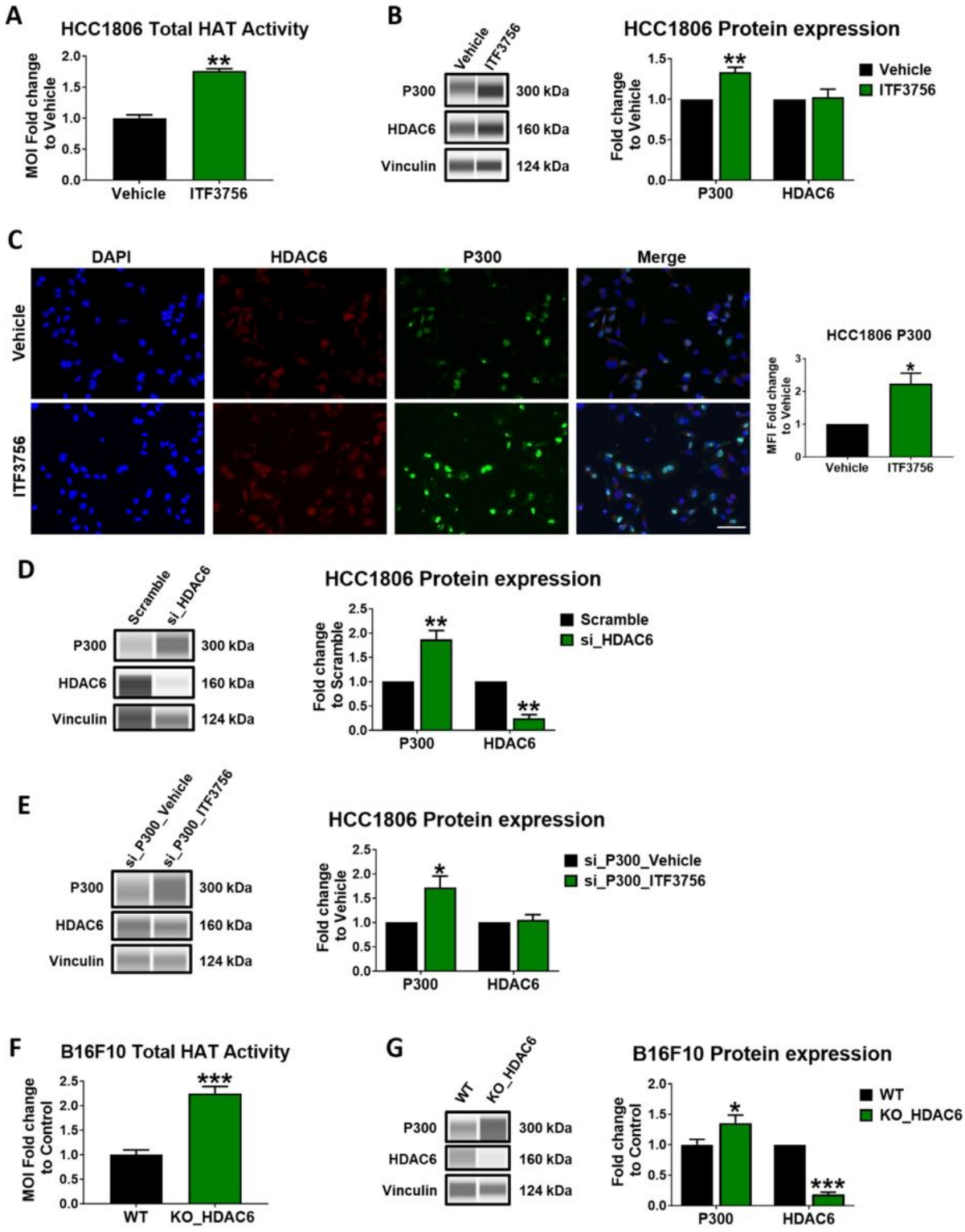

Figure 2

HDAC6 inhibition/inactivation increases total HAT activity and P300 protein level. (**A**) Total HAT activity assay was performed in the HCC1806 cell line, comparing ITF3756 1 μM 16h treatment (green bar) and the control condition (black bar). Error bars indicate SEM. Data were analyzed by paired t-test, N=3; **p<0.005. (**B**) P300 and HDAC6 protein expression. Left: representative image showing P300 and HDAC6 proteins in the HCC1806 cell line. Right: graph reporting the mean protein levels. Vinculin was used as a

normalizer. Error bars indicate SEM. Multiple comparison 2-way ANOVA was used to analyze the data, N=5; **p<0.005. (**C**) Immunofluorescence staining. Left: representative images showing P300 (green signal) and HDAC6-Flag (red signal) in the HCC1806 cell line after 24h of pCDNA3_HDAC6Flag transfection and 16h treatment with 1 µM ITF3756. DAPI (blue signal) was used as a normalizer. Images were acquired at 20X magnification. Scale bar: 100 µm. Right: densitometric analysis of the Mean Fluorescent Intensity (MFI). Error bars indicate SEM. Data were analyzed by paired t-test, N=3; *p<0.05. (**D, E**) HDAC6 and P300 silencing. Left: representative capillary electrophoresis experiments showing P300 and HDAC6 protein levels after HDAC6 or P300 silencing. Right: mean protein levels of P300 and HDAC6. Vinculin was used as a normalizer. Error bars indicate SEM. Multiple comparison 2-way ANOVA was used to analyze the data, N=3; *p<0.05; **p<0.005. (**F**) Total HAT activity in the B16F10 cell line (HDAC6_KO, green bar, *vs*WT, black bar). Error bars indicate SEM. Data were analyzed by unpaired t-test, N=4; ***p<0.0005. (**G**) Left: representative capillary electrophoresis experiment showing P300 and HDAC6 proteins in B16F10 cells. Right: mean protein levels of P300 and HDAC6. Vinculin was used as a normalizer. Error bars indicate SEM. Multiple comparison 2-way ANOVA was used to analyze the data, N=4; *p<0.05; ***p<0.0005.

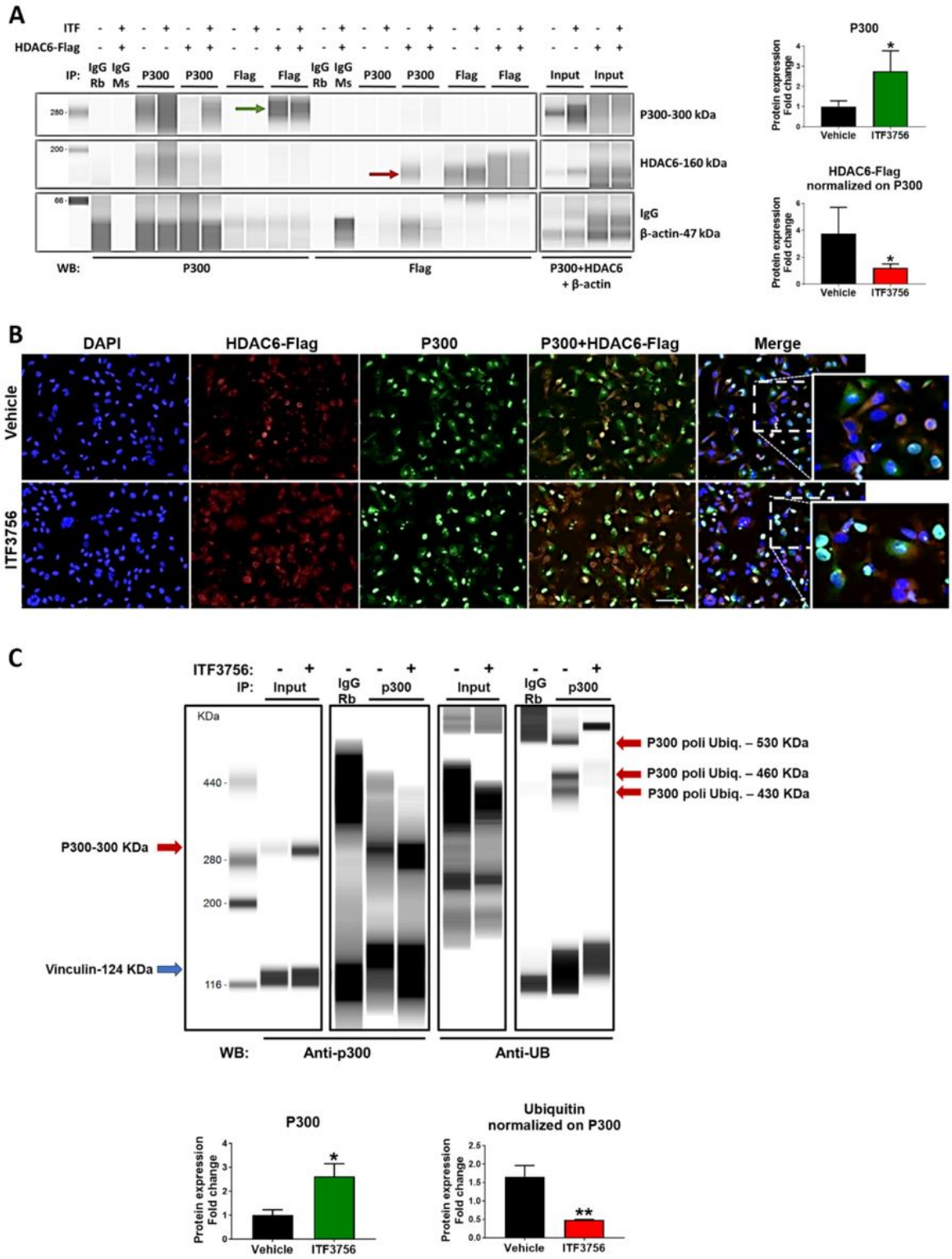

Figure 3

ITF3576 interferes with HDAC6/P300 association. (**A**) Left: Co-Immunoprecipitation capillary electrophoresis experiments were performed on HEK293T cells transfected with pCDNA3.1+_HDAC6_Flag and pCDNA3.1+ as a control for 24h and treated with 1 μM ITF3756 for an additional 16h; DMSO was used as solvent control. The arrows indicate a decreased P300-HDAC6 interaction upon ITF3756 treatment. Right, top: mean protein levels of free P300 upon ITF3576 or vehicle treatment and

immunoprecipitation with an anti-P300 antibody in pCDNA3.1+_HDAC6_Flag-transfected cells. Right, bottom: HDAC6-Flag protein levels upon ITF3576 or vehicle treatment and immunoprecipitation with an anti-Flag antibody in pCDNA3.1+ _HDAC6_Flag-transfected cells-, normalized on respective P300 content. Error bars indicate SEM. Data were analyzed by unpaired t-test, N=3; *p<0.05. (**B**) Immunofluorescence. Representative images showing P300 (green signal) and HDAC6-Flag (red signal) in the HCC1806 cell line after 24h of pCDNA3_HDAC6_Flag transfection and 16h of treatment with 1 μM ITF3756. DAPI (blue signal) was used as normalizer. Images were acquired at 20X magnification. Scale bar: 100 μm. (**C**) ITF3576 impairs P300 ubiquitination. Top: capillary electrophoresis experiments were performed on HCC1806 cells treated with 1 μM ITF3756 for 16h compared to solvent control. Samples were immunoprecipitated with an anti-P300 antibody, and blotted with an anti-P300 antibody (on the middle left) and with an anti-polyubiquitin antibody (on the right). Arrows on the left indicate P300 (red) and the normalizer Vinculin (blue). The red arrows on the right show the P300 polyubiquitinated species. Bottom, left: P300 mean protein levels in ITF3756-treated cells (green bar) compared to solvent (black bar), measuring samples immunoprecipitated and blotted with anti-P300 antibody. Bottom, right: quantification of the mean content of the P300 ubiquitinated species, measuring samples immunoprecipitated with anti-P300 antibody and blotted with anti-polyubiquitin antibody, in cells treated with ITF3756 (red bar) compared to the control (black bar), and normalized on the respective P300 amount. Error bars indicate SEM. Data were analyzed by unpaired t-test, N=3; *p<0.05.

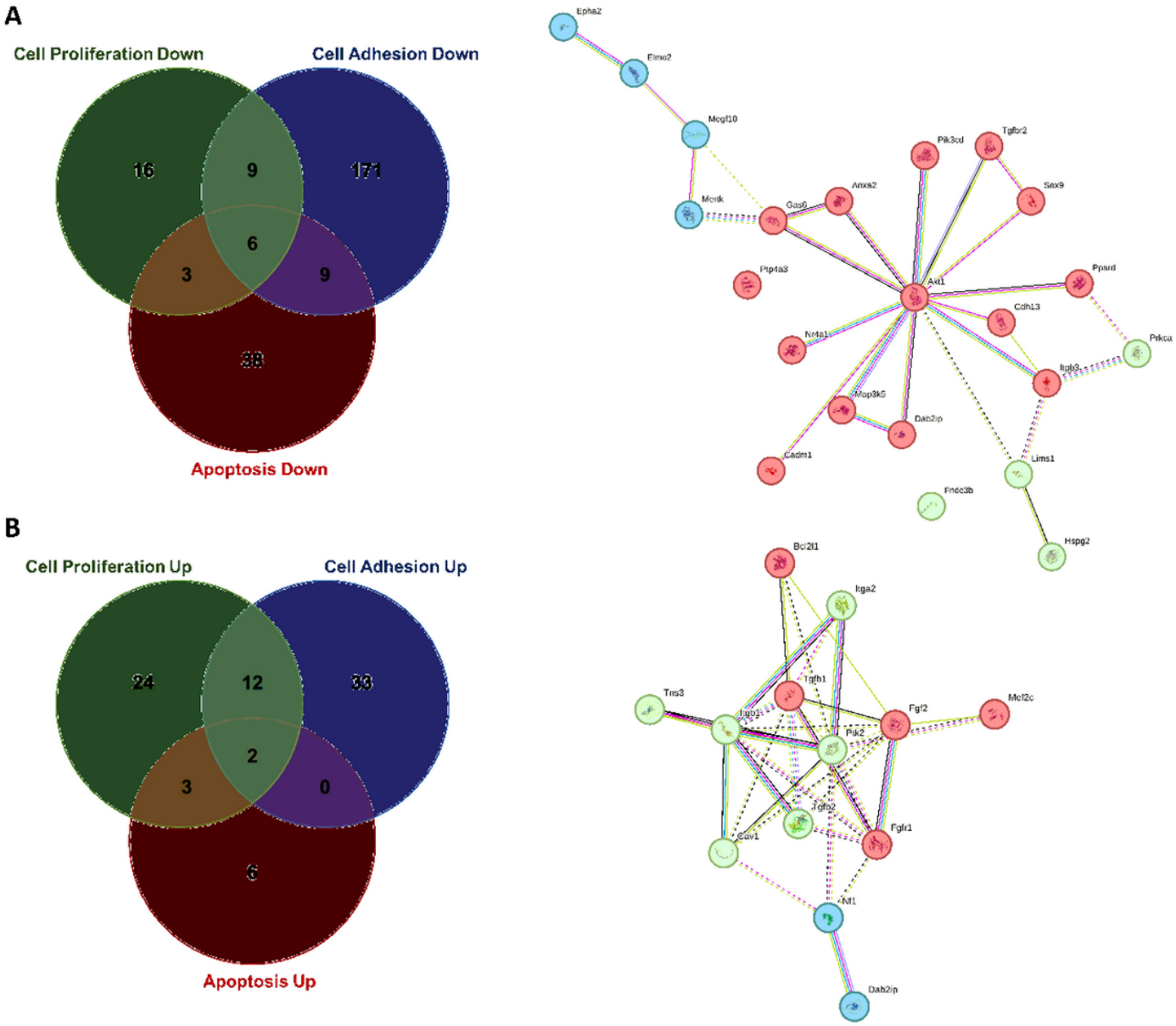

Figure 4

ATAC-seq and H3K27Ac-ChIP-Seq integrated analysis in KO_HDAC6 *vs* WT B16F10 cells. (**A**) Venn diagram (left) and Gene network analysis (right) show the intersection between down-regulated genes identified by ATAC-seq and H3K27Ac-ChIP-seq analysis associated with cell proliferation, cell adhesion, and apoptosis. (**B**) Venn diagram (left) and Gene network analysis (Right) show the intersection between up-regulated genes identified by ATAC-seq and H3K27Ac-ChIP-seq analysis associated with cell proliferation, cell adhesion, and apoptosis.

Supplementary Files

This is a list of supplementary files associated with this preprint. Click to download.

- SupportingInformationforMGZSR.docx